PHOTOEMISSION ELECTRON MICROSCOPY STUDY OF SUB-200 nm SELF-ASSEMBLED $La_{0.7}Sr_{0.3}MnO_3$ EPITAXIAL ISLANDS

Jone Zabaleta,[*a] Sergio Valencia,[b] Florian Kronast, [b] César Moreno,[a,c] Patricia Abellán,[a,d] Jaume Gázquez,[a] H. Sepehri-Amin,[c] Felip Sandiumenge, [a,] Teresa Puig, [a,] Narcís Mestres [a,] and Xavier Obradors [a,]

[a] *ICMAB-CSIC,Campus de la UAB, 08193 Bellaterra, Spain.*
[b] *Helmholtz-Zentrum Berlin, Albert-Einstein-Strasse 15, D-12489, Berlin, Germany.*
[c] *International Center for Young Scientists, National Institute for Materials Science, Tsukuba 305-0047, Japan*
[d] *Chem. & Matrls. Sci. Div., Pacific Northwest National Laboratory, Richland, WA 99352 USA*

*Presently at *Max Planck Institute für Festkörperforschung, Heisenbergstr. 1, 70569 Stuttgart, Germany; E-mail:J.Zabaleta@fkf.mpg.de; jone.zabaleta@gmail.com*

FURTHER EXPERIMENTAL DETAILS

Nanoisland Synthesis

$La_{0.7}Sr_{0.3}MnO_3$ (LSMO) nanostructures were grown using the Chemical Solution Deposition (CSD) methodology, following an all-propionate route first developed by Hasenkox et al. [1]. Stoichiometric amounts of the metal propionates are mixed in propionic acid to obtain precursor solutions of 0.3 M concentration (with respect to Mn), which are further diluted down to 0.03 M. The metalorganic solution is then deposited on 5 x 5 mm^2 fluorite-structure (001)-oriented yttria-doped ZrO_2 single crystal substrates and spin-coated at 6000 rpm for 2 min. The gel is finally heated at 900 °C under flowing O_2 (0.6 l min^{-1}) for 1 h. During this annealing the organic matter decomposes and LSMO crystalline structures build-up in the form of self-assembled epitaxial nanostructures [2].

Technical Details

Atomic Force Microscopy topography measurements were performed in the dynamic mode at room temperature and ambient atmosphere using an Agilent 5100 (Molecular Imaging).

X-ray diffraction measurements were done with a GADDS D8 Advance system from Bruker with a 2D-detector.

Cross-sectional specimens were prepared for TEM examination by using the mechanical tripod polisher technique followed by Ar ion milling at 3.5 KeV down to perforation in a Precision Ion Polishing system. TEM images were acquired with a 200 KV Jeol 2010F microscope, while electron diffraction patterns were obtained using a 300 KV Philips CM30.

A Superconducting Quantum Interferometer Device (SQUID) magnetometer (Quantum Design MPMS-XL7) was used for the magnetization measurements of the LSMO nanoislands. Magnetization (*M*) versus magnetic field (*H*) loops were measured for a set of different temperatures from 10 K to 300 K and varying magnetic fields between 0 and ±7 T. The substrate diamagnetic response (*M* linear dependency against *H)* was subtracted in order to extract the ferromagnetic (FM) behavior specific to the LSMO nanoislands. *M* versus temperature curves showed *Tc* values of around ~350 K [2].

Photoemission Electron Microscopy (PEEM) imaging was performed at the undulator beamline UE49PGM of the synchrotron light source Bessy II in Berlin, Germany. The x-ray source is an elliptical undulator with polarization control .The PEEM is based on a Elmitec III instrument, with energy resolution (E/ΔE) of 10000 at 700 eV. The sample holder used for PEEM imaging allowed for the application of a uniaxial in-plane magnetic field up to 70 mT as well as for the cooling down to a base temperature of 110 K.

MICROMAGNETIC FINITE ELEMENT SIMULATIONS

To study the different switching magnetic behavior of the small islands (e.g. island no. 10 in Figure 5 or 6 of the manuscript) compared to the large islands (e.g. islands no. 2,3,4 or 8) 3D finite element micromagnetic simulations were performed on cuboid shaped models with different dimensions from 20×10×20 nm^3 to 200×30×200 nm^3. Tetrahedron meshes were applied on the models with a size of 2 nm and the Landau-Lifshitz-Gilbert equation at each node was solved by the FEMME software [3]. The saturation magnetization ($\mu_0 M_s$), the magnetocrystalline anisotropy (K_1) and the exchange stiffness (A) of the LSMO were chosen to be 0.7 T, -5 kJ m^{-3} and 5 pJ m^{-1}, respectively [2]. The magnetic field was applied parallel to Z direction from +1T to -1 T. Single domain structure was found during the whole magnetization process with a coherent rotation magnetization and reversal process for modeled nanocrystalline microstructures with dimensions smaller than 50×50 nm^2 area and 15 nm thickness. In contrast, multidomain behavior, with vortex states, was found for modeled samples with a dimension from 50×15×50 nm^3 to 200×30×200 nm^3. Full frame movies covering the magnetization and magnetization reversal of modeled samples with a size of 40×10×40 nm^3 and 100×30×100 nm^3 are shown in the supplementary files.

Figure S1 shows the hysteresis loops of simulated models for a typical small structure (40×10×40 nm^3) and a large structure (100×30×100 nm^3) with their main frames of interest displayed below. Note that the coercivity obtained in the micromagnetic simulation result is higher than that of experimentally obtained data. One possible reason can be due to existing surface defects in the islands causing deviation of the magnetocrystalline anisotropy compared to the theoretical value which was used in the micromagnetic simulation. The other possible reason can be due to the difference between the real shapes of islands and the cuboid shape assumed in the simulation. The red and blue contrast in the 3D simulations indicate the direction of the magnetization in the +Z and −Z directions. On the left side image series we show the magnetization reversal process for a large structure displaying multidomain configuration and the formation of a magnetic vortex. In contrast, for small structures we observe a single domain configuration during the magnetization reversal process.

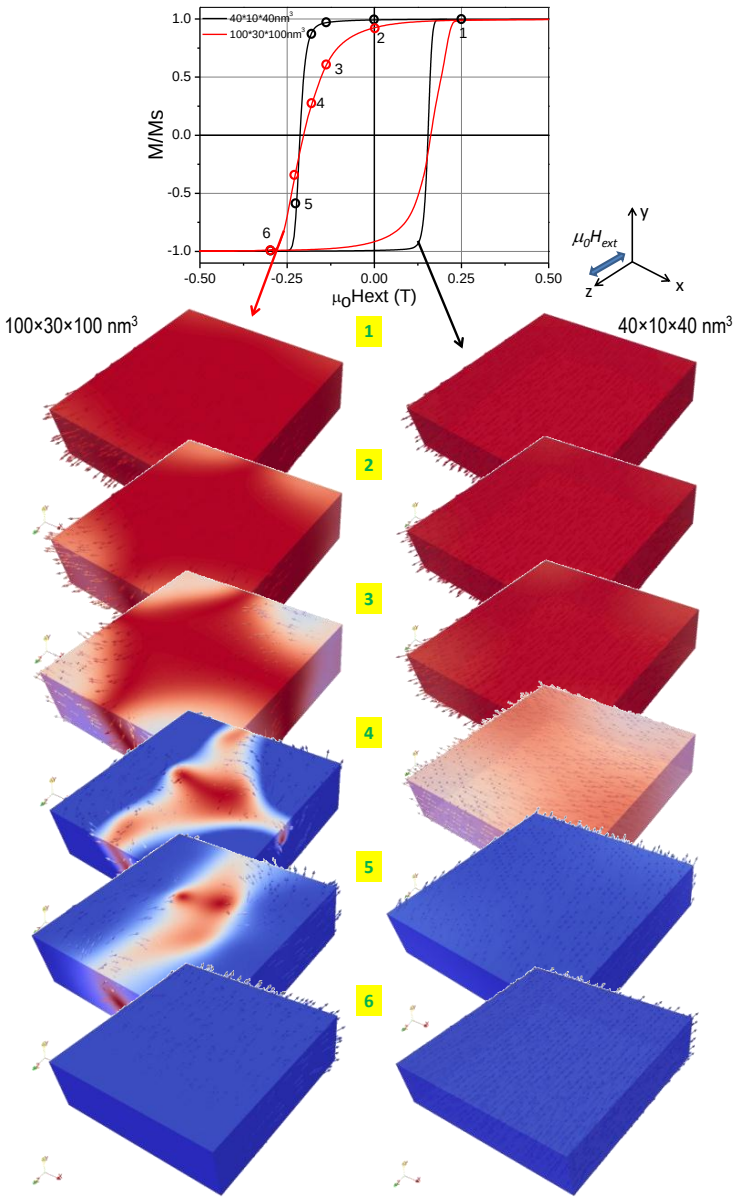

Fig. S1: (Top panel) Magnetization curve of the modeled islands with size 100×30×100 nm^3 (red line) and 40×10×40 nm^3 (black line). (Bottom panel) Magnetization configuration of the two modeled samples. The results for applied magnetic fields of 0.25 T, 0.0 T, -0.12 T, -0.20 T, -0.23 T, and -0.28 T are shown through point 1 to 6. For the large island (thickness 30 nm) the magnetization reversal shows a multidomain structure while for the small island (thickness 10 nm) a single domain structure is detected at every stage during the magnetization reversal.

ASSESSING THE SUITABILITY OF THE METAL CAPPING

The capping of the self-assembled LSMO nanoislands (grown on an insulating substrate) with a conducting layer is the major limiting experimental factor one has to deal with in the case of small objects such as our sub-200 nm structures. Reaching the compromise between conductivity and measurable signal from the buried nanostructures is key to enabling both XAS and XMCD investigations.

Pt was selected as the final capping material among other metals because it is a good electrical conductor (therefore allowing for thinner capping) and chemically inert. The low oxidation potential of Pt

(-1.188 eV), only higher than Au (-1.52 eV), makes it a good choice for deposition onto an oxide such as our LSMO, since it makes the LSMO de-oxygenation highly unlikely. Previous works have also ascertained the inertness of Pt on LSMO [4]. The main drawback of Pt is the small electron mean escape depth (Δ), compared for example to Al or Cu. A low Δ value makes it hard for electrons leaving the LSMO to traverse the Pt capping. This is the reason why we also investigated these two metals, i.e. Al and Cu, which are more transparent to electrons. In particular, the inelastic mean free path of electrons, λ_i, is largest in Al, then in Cu, and smallest in Pt (λ_i, depends on Δ) [5]. However, the strong tendency of Al towards oxidation (its oxidation potential is the highest of all elemental metals except K, Ca, Na and Mg) can trigger depletion of oxygen from the LSMO upper layers, with the consequent loss of ferromagnetism [6]. To avoid this from happening 1.5 nm Cu were deposited, in-situ, prior to Al evaporation. The XAS done on Cu(1.5nm)/Al(5nm) coated LSMO nanoisland samples. Nevertheless, Figure S2 shows a massive generation of Mn^{2+} which forms in detriment of stoichiometric LSMO as consequence of LSMO de-oxygenation. Such XAS spectra are in agreement with Mn^{2+} XAS spectra from the literature [7], and in clear contrast with the XAS spectra shown for Pt coated LSMO nanoisland samples (Figure 3 of the manuscript), where the peak related to Mn^{2+} , detected on the surface spectra, coexists with features specific to Mn^{3+}/Mn^{4+}. As expected, no XMCD signal was detected in Cu/Al- coated samples, again in contrast to the Pt-coated samples investigated in the manuscript. For its part, Cu deposition resulted in an inhomogeneous distribution of the metal resulting in the charging of the sample. The inertness of Pt and its low oxidation potential make it unlikely that it should be the promoter of our detected Mn^{2+} signal. Evidence of Mn^{2+} in non-coated LSMO samples in the literature also support this point [8].

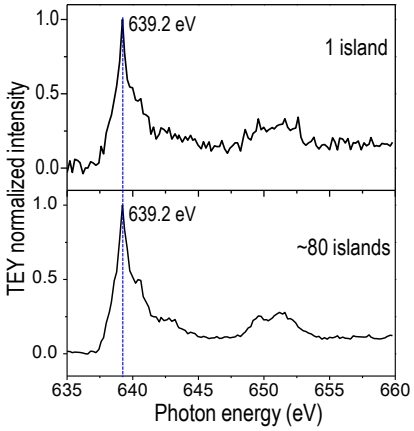

Fig. S2: XAS of the Mn $L_{2,3}$ -edges for a 1.5 nm Cu/5 nm Al coated LSMO nanoisland sample. Spectra for 1 island and 80 islands are shown. The integration of many nanoislands largely increases the signal to noise ratio and results in a spectrum characteristic of Mn^{2+} in agreement with the literature [7].

Uniformity of the Pt capping

The Pt capping is uniform and homogeneous, as demonstrated by atomic force microscopy (AFM) topography data. Figure S3 shows a topography image of a self-assembled LSMO nanoisland sample before Pt capping and Figure S4 shows the same sample after Pt was deposited to achieve a conducting surface. The topography of the islands is essentially the same after Pt deposition, but for a slight widening and rounding of the island edges due to material deposition. Also, the substrate surface- island relative height is maintained in both samples, as shown by the representative line scans and also by the height bar scales of Figure S3 and Figure S4. The only indication of the presence of deposited material was found in very few areas such as the one in the upper left side of Figure S4(a), which

shows slight irregularities. Besides, in case of detecting any capping anomaly during PEEM measurements this could be easily avoided by moving to a different area of the sample, since PEEM is a spatially resolved technique. It should be nevertheless noted that, although homogeneous and uniform, we cannot discard subtle variations in the Pt thickness from one spot to the other, which could be in the order of a few angstroms. These slight variations will influence the amount of electrons escaping the Pt and thus the intensity of the signal measured by PEEM.

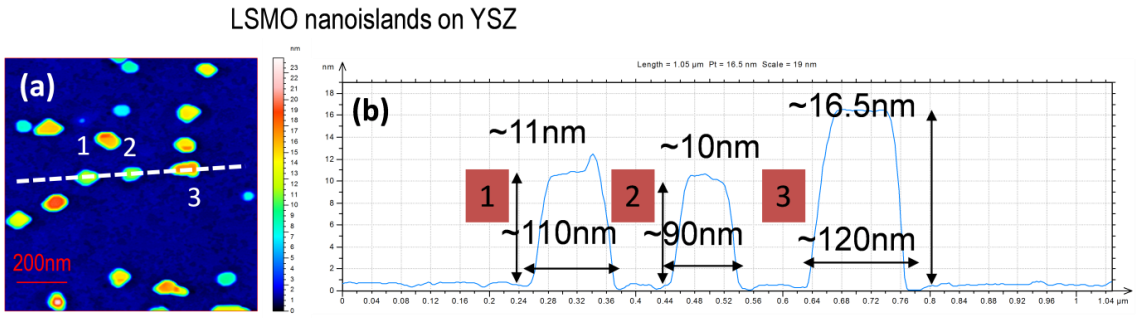

Fig. S3: Topography AFM image (a) and its corresponding line scan (b) of a system of self-assembled LSMO nanoislands on YSZ.

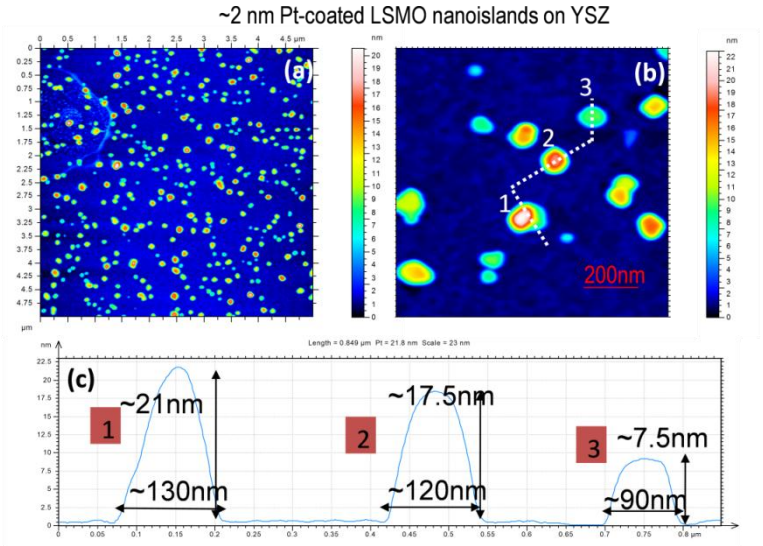

Fig. S4: Topography AFM images (a) & (b), and a corresponding line scan (c) of the same system of self-assembled LSMO nanoislands on YSZ as in Figure S3, but after ~2 nm Pt were deposited.

ASSESSING THE EFFECT OF IRRADIATION ON THE CHEMISTRY AND MAGNETISM OF LSMO NANOISLANDS

We did not observe any change in the chemical spectra with X-ray beam exposition time, which includes no change in the Mn^{2+} signal. If we compare the Mn L-edge XAS features of a group of nanoislands at a certain time t_1 (the spectrum took ~15 min to be completed) and ~45 min after continuously irradiating the same spot, we observe no relevant differences (Figure S5). This is also in agreement with the fact that no magnetic signal loss was observed after ~45 min of steady irradiation (Figure S6). Note that the signal-to-noise ratio in the surface spectra in Figure S5 (the *absorption* spectra) is low because we only show the result of one individual spectrum at t_1 and another single spectrum 45 min later (in order to evaluate evident chemical changes with irradiation time). To achieve better signal-to-noise ratio we had to average multiple spectra, which also made the Mn^{2+}

traces more visible (e.g. Figure 3d of the manuscript). The XMCD contrast in the snapshots of Figure S6(a), for its part, is extremely weak because the measurement was done at 300 K (the magnetization value at room temperature is low) and because they are single images. In order to enhance signal-to-noise ratios we would average all the images done (a total of 7), as shown in Figure S6(b). Anyhow, Figure S6(a) already shows that the fluctuations in the (small) magnetic signal do not follow a monotonic decrease which could be associated with a loss of magnetism.

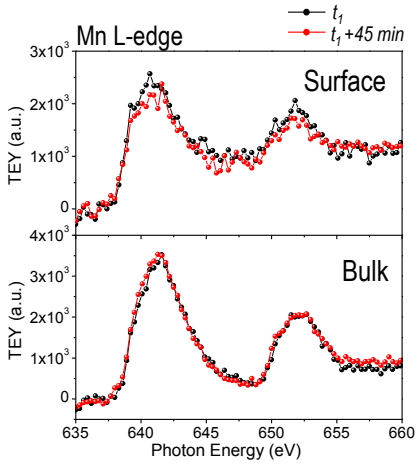

Fig. S5: Mn L-edge XAS of a LSMO nanoisland ensemble after X-ray irradiation during ~15 min (t_1, black) and ~60 min (t_1+ 45, red). The spectra exhibit no appreciable variations.

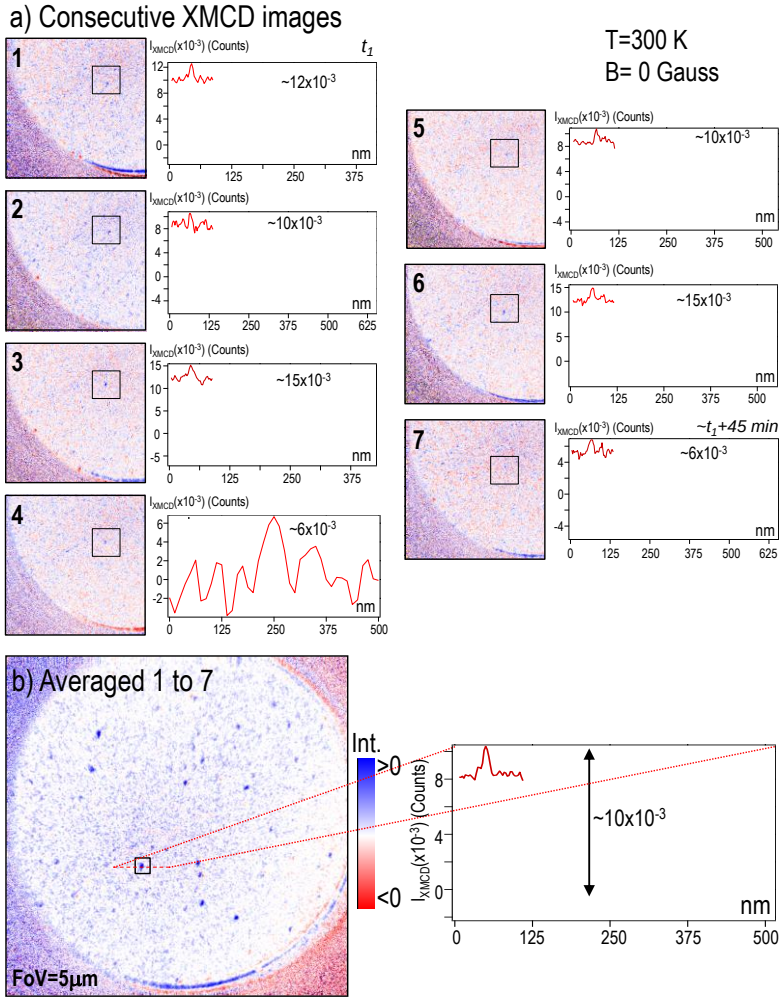

Fig. S6: XMCD images, taken at the Mn L_3-edge, of self-assembled LSMO islands at T=300K and B=0 Gauss.

(a) A set of chronologically ordered XMCD images. The accompanying line-scans express the intensity evolution of the XMCD contrast with time corresponding to a single island (marked within black squares). (b) The result of averaging the 7 images.

References

[1] U. Hasenkox, C. Mitze, and R. Waser, *Metal propionate synthesis of magnetoresistive* $La_{1-x}(Ca,Sr)_x\ MnO_3$ *thin films,* J. Am. Ceram. Soc. 80, 2709 (1997).

[2] J. Zabaleta, M. Jaafar, P. Abellan, C. Monton, O. Iglesias-Freire, F. Sandiumenge, C. A. Ramos, R. D. Zysler, T. Puig, A. Asenjo, N. Mestres and X. Obradors, *Nanoscale magnetic structure and properties of solution-derived self-assembled* $La_{0.7}Sr_{0.3}MnO_3$ *islands,* J. App. Phys. 111, 024307 (2012)

[3] T. Schrefl, J. Fidler, *Micromagnetic simulation of magnetizability of nanocomposite Nd–Fe–B magnets* J. Appl. Phys. 83, 6262 (1998)

[4] Z.-T Xu, K.-J. Jin, C. Wang *et al*, *Unusual resistive switching induced by voltage in* $La_{0.7}Sr_{0.3}MnO_3$, Appl. Phys. A, (2011)

[5] C. J. Powell and A. Jablonski, *Surface sensitivity of X-ray photoelectron spectroscopy*, Nucl. Instrum. Methods Phys. Res., Sect. A 601, 54 (2009).

[6] S. Stadler, Y. U. Idzerda, Z. Chen, S. B. Ogale, and T. Venkatesan, *The magnetism of a buried* $La_{0.7}\ Sr_{0.3}\ MnO_3$ *interface*, Appl. Phys. Lett. 75, 3384 (1999).

[7] F. M. F. de Groot, J. C. Fuggle, B. T. Thole, and G. A. Sawatzky, *2p x-ray absorption of 3d transition-metal compounds: An atomic multiplet description including the crystal field*, Phys. Rev. B 42, 5459 (1990); C. Mitra, Z. Hu, P. Raychaudhuri *et al., Direct observation of electron doping in* $La_{0.7}Ce_{0.3}\ MnO_3$ *using X-ray absorption spectroscopy*, Phys. Rev. B 67,092404 (2003).

[8] S.Valencia *et al*. Phys. Rev. B **73**, 104402 (2006); S. Valencia *et al*. Phys. Rev. B **75**, 184431 (2007)